First search for axion dark matter with a MADMAX prototype

MADMAX Collaboration: B. Ary dos Santos Garcia,[1] D. Bergermann,[1] A. Caldwell,[2] V. Dabhi,[3] C. Diaconu,[3] J. Diehl,[2] G. Dvali,[2] J. Egge,[4] E. Garutti,[4] S. Heyminck,[5] F. Hubaut,[3] A. Ivanov,[2] J. Jochum,[6] S. Knirck,[7] M. Kramer,[5] D. Kreikemeyer-Lorenzo,[2] C. Krieger,[4] C. Lee*,[2] D. Leppla-Weber,[8] X. Li†,[2] A. Lindner,[8] B. Majorovits,[2] J.P.A. Maldonado,[2] A. Martini,[8] A. Miyazaki,[9] E. Öz,[1] P. Pralavorio,[3] G. Raffelt,[2] J. Redondo,[10] A. Ringwald,[8] J. Schaffran,[8] A. Schmidt,[1] F. Steffen,[2] C. Strandhagen,[6] I. Usherov,[6] H. Wang,[1] and G. Wieching[5]

[1] *III. Physikalisches Institut A, RWTH Aachen University, Aachen, Germany*
[2] *Max-Planck-Institut für Physik, Garching, Germany*
[3] *Aix Marseille Université, CNRS/IN2P3, CPPM, Marseille, France*
[4] *Universität Hamburg, Hamburg, Germany*
[5] *Max-Planck-Institut für Radioastronomie, Bonn, Germany*
[6] *Physikalisches Institut, Eberhard Karls Universität Tübingen, Tübingen, Germany*
[7] *Fermi National Accelerator Laboratory, Batavia, USA*
[8] *Deutsches Elektronen-Synchrotron DESY, Notkestr. 85, 22607 Hamburg, Germany*
[9] *Université Paris-Saclay, CNRS/IN2P3, IJCLab, Orsay, France*
[10] *Universidad de Zaragoza, Zaragoza, Spain*

This paper presents the first search for dark matter axions with mass in the ranges 76.56 to 76.82 µeV and 79.31 to 79.53 µeV using a prototype setup for the MAgnetized Disk and Mirror Axion eXperiment (MADMAX). The experimental setup employs a dielectric haloscope consisting of three sapphire disks and a mirror to resonantly enhance the axion-induced microwave signal within the magnetic dipole field provided by the 1.6 T Morpurgo magnet at CERN. Over 14.5 days of data collection, no axion signal was detected. A 95% CL upper limit on the axion-photon coupling strength down to $|g_{a\gamma}| \sim 2 \times 10^{-11}\text{GeV}^{-1}$ is set in the targeted mass ranges, surpassing previous constraints, assuming a local axion dark matter density ρ_a of 0.3 GeV/cm^3. This study marks the first axion dark matter search using a dielectric haloscope.

Introduction—Axions have become prominent candidates for cold dark matter (DM) [1–4]. They were originally introduced to explain the absence of CP-violating effects in quantum chromodynamics (QCD) through the Peccei-Quinn (PQ) mechanism [5–8]. In the well motivated post-inflationary PQ-symmetry breaking scenario the axion mass required to match the observed DM density is expected to be in the range $m_a \sim 40$ to 180 µeV [9]. In the following, the term axion will refer to both, QCD axions and axion-like particles.

In an external magnetic field $\mathbf{B}_e$, axions convert to photons and source an oscillating current with frequency corresponding to m_a, given by $\mathbf{J}_a = g_{a\gamma}\mathbf{B}_e\dot{a}$ [10], with $g_{a\gamma}$ the axion-photon coupling strength and $\dot{a}$ the temporal derivative of the axion field. Cavity searches are a promising approach to detect axions [11]. They are designed to convert axions from the DM halo into microwave photons using a resonator in a magnetic field. Several cavity searches [12–18] have already put significant constraints on $|g_{a\gamma}|$ for $1\,\mu\text{eV} \lesssim m_a \lesssim 40\,\mu\text{eV}$, with first efforts being underway to test higher m_a [19–21], which are challenging to probe with cavity experiments as their size must be adjusted to match the wavelength of the generated photon. At higher m_a values, corresponding to higher frequencies of the generated photon, this results in a reduced volume for resonant axion-photon conversion, thereby decreasing sensitivity.

The MAgnetized Disk and Mirror Axion eXperiment (MADMAX) [22–24] makes use of the dielectric haloscope concept to access the well-motivated mass range $m_a > 40\,\mu\text{eV}$. This concept, based on the magnetized mirror axion DM search idea [25], uses a *booster* composed of a set of parallel dielectric disks and a metallic mirror to enhance a potential axion signal, effectively decoupling the conversion volume from the wavelength and thereby overcoming the limitation of typical cavity experiments towards higher masses.

Due to the large de Broglie wavelength of the considered non-relativistic DM axions of $\mathcal{O}(10\,\text{m})$, $\mathbf{J}_a$ is assumed to be uniform over the extent of the booster. This leads to an oscillating electric field uniform across a single medium with dielectric permittivity ϵ. The field $\mathbf{E}_a$ exhibits discontinuities at the boundaries of different media, resulting in the emission of traveling waves with frequency corresponding to m_a ensuring the continuity of the total electric field. The signal power P_{sig} due to the coherent emission from multiple surfaces in relation to the power emitted by an ideal magnetized mirror, P_0, is enhanced by the frequency dependent boost factor $\beta^2 = P_{\text{sig}}/P_0$. By adjusting the disk positions its center frequency and width can be tuned. This makes it possible to boost the potential DM axion signal compared to the magnetized mirror concept [25] in dedicated mass ranges. The sensitivity of a MADMAX prototype setup to

*Now at LLNL, Livermore, CA, USA
†Now at TRIUMF, Vancouver, Canada

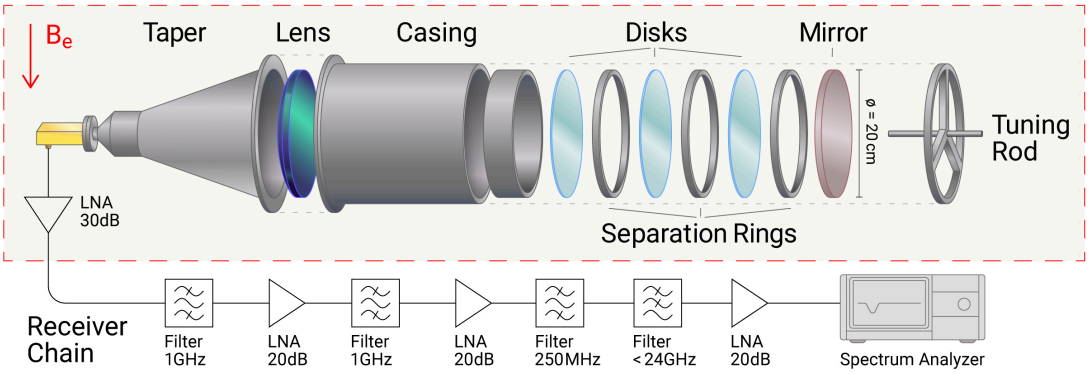

Figure 1: Exploded schematic view of the MADMAX prototype CB200 and the receiver chain. The shaded region represents the components exposed to the B-field.

$|g_{a\gamma}|$ for a specific signal to noise ratio (SNR) is [10]

$$|g_{a\gamma}| = 4\times10^{-11}\,\mathrm{GeV}^{-1}\sqrt{\frac{2\times10^3}{\beta^2}}\sqrt{\frac{T_{\mathrm{sys}}}{300\,\mathrm{K}}} \times\left(\frac{0.1\,\mathrm{m}}{r}\right)\left(\frac{1\,\mathrm{T}}{B_e}\right)\left(\frac{1.3\,\mathrm{days}}{\Delta t}\right)^{1/4}\sqrt{\frac{\mathrm{SNR}}{5}} \times\left(\frac{m_a}{80\,\mu\mathrm{eV}}\right)^{5/4}\sqrt{\frac{0.3\,\mathrm{GeV/cm^3}}{\rho_a}}\,, \quad (1)$$

with system temperature T_{sys}, radius r of the disks and mirror, effective data-taking time Δt, and the local axion DM density ρ_a.

The MADMAX Collaboration has made significant progress in advancing the development of a future large-scale dielectric haloscope [26–33]. Small-scale setups have successfully validated the dielectric haloscope approach in dark photon DM searches [34, 35], specifically with a broadband MADMAX prototype [35]. Here we demonstrate for the first time tunability in a MADMAX prototype. By combining a prototype booster with an external dipole magnetic field, it marks the first axion DM search using a dielectric haloscope, probing previously unexplored parameter space.

Experimental Setup—To perform the axion search, the Closed Booster 200 (CB200) MADMAX prototype is used. As illustrated in Fig. 1, it consists of an aluminum mirror and three sapphire circular disks of 1 mm thickness, each with a diameter of 200 mm and distanced by separation rings enclosed in an aluminum casing, a Rexolite© microwave lens and an aluminum taper, all controlled at $\mathcal{O}(10\,\mu\mathrm{m})$ precision [33]. In contrast to the design used in Ref. [35] and envisioned for the MADMAX design, the prototype is enclosed by conductive boundaries, resulting in fixed boundary conditions, such that only a limited number of cylindrical wave-guide modes within a given frequency range exists inside the booster. This significantly simplifies modelling of the electromagnetic response and allows to determine the boost factor with fewer dedicated measurements. Approximately 84% of the axion induced power couples to the fundamental transverse electric TE_{11} mode as calculated by the modal overlap formalism. The emitted TE_{11} power emissions are coupled into the receiver chain by a lens and a taper specifically designed for this via a 50 Ω transmission line. The power output of the system is coupled to a heterodyne receiver system, consisting of a series of low noise amplifiers (LNAs) and filters, and a Rohde & Schwarz FSW43 real-time spectrum analyser (SA), which streams time-domain data to a computer where it is Fourier transformed on GPUs with ∼0.11 s coherent integration length. The resulting power spectra are averaged in batches of 8047 single spectra, corresponding to roughly 15 min measurement time each. The receiver system has a bandwidth of ∼ 250 MHz, which is approximately centred around the respective boost factor peak, a resolution of 9 Hz and provides negligible dead-time. It was configured for each run to acquire data around the frequency of the expected maximum boost factor. A Y-factor method [36] is adopted to calibrate the output of the receiver system to system temperature T_{sys}. T_{sys} is dominated by the higher than expected noise of the receiver chain of ∼ 230 K. (Pictures of the full setup can be found in Fig. S1 of the suppl. material.)

Two different disk spacing *configurations* were used to search for axions: Configuration 1 is designed to be sensitive around 18.55 GHz and Configuration 2 around 19.21 GHz, corresponding to axion masses around 76.72 µeV and 79.45 µeV, respectively. Frequency adjustment is done by proper choice of the width of separation rings between adjacent disks and between mirror-facing disk and mirror: 12.52 mm, 12.25 mm and 8.38 mm (from left to right in Fig. 1) for configuration 1 and 11.89 mm, 12.25 mm and 8.02 mm for configuration 2. The widths are optimized for a resonance of the TE_{11} mode between mirror and adjacent disk. A $\mathcal{O}(\mu\mathrm{m})$ change in separation between mirror and closest disk results in $\mathcal{O}(\mathrm{MHz})$ frequency shift of the boost factor distribution. The peak frequencies for both configurations were precisely

tuned for different runs to different values by applying mechanical force to the mirror using an adjustable metal tuning rod. Three *physics-runs* around 18.55 GHz and two around 19.21 GHz were performed, sensitive to different frequency ranges with peak frequencies separated by ~ 10 MHz.

Measurements of CB200 power spectra with a total measurement time of 14.5 days have been performed inside the Morpurgo dipole magnet [37] at CERN. The magnet was operated at field strengths from 1 to 1.58 T (see Table S1 and Fig. S2 in suppl. material).

Boost factor determination—β^2, which is strongly correlated to the reflectivity S_{11} of the system [10], and its corresponding uncertainties are determined using a one-dimensional booster model implemented in ADS [48]. The model is fitted to S_{11} measurements of the booster. Disk positions, thicknesses, dielectric losses and permittivity are extracted. They are within their measurement uncertainties. Losses due to three-dimensional effects, such as tilts, are modelled by effective dielectric losses.

Identification of the TE_{11} booster mode is done for each configuration by measuring the shape of the E-field between mirror and closest disk, using a bead-pull method [30]. It follows the expected shape (see Figs. S3 and S4 in suppl. material). S_{11} measurements confirm the separation of the TE_{11} modes from parasitic modes.

The boost factor is reduced by a factor 0.84 when taking into account the overlap of the three-dimensional field shape with the uniform axion current. This is analogous to a form factor in cavity experiments. The uncertainty on the overlap of $\pm 10\%$ is determined from the deviation between expected and measured field shape obtained from bead-pull measurements.

When measuring power spectra, the $\sim 41.5\,\Omega$ impedance of the first LNA of the receiver chain leads to a mismatch with the transmission line inducing a standing wave between booster and LNA. This modifies the boost factor obtained from S_{11} measurements, depending on the distance between the booster and this LNA. The latter is determined from the broadband oscillation pattern induced by resonance of the LNA noise, similar as in [35]. The modelled frequency behavior of the power spectra, adapted to consider the LNA impedance mismatch, match the measured ones from the physics-runs. (See Figs. S5 and S6 in suppl. material for more details.) Broadband power spectra measurements were taken prior to each physics-run. Any drifts in $T_{\rm sys}$ or frequency are obtained in situ from the physics runs. The variation of the measured peak frequency values during physics runs is used to evaluate the systematic uncertainty on β^2. It follows a Gaussian distribution with a width around 200 kHz for all physics-runs, resulting in an additional uncertainty in β^2 for a given frequency of less than 1%.

The extracted boost factors including their uncertainties are shown in Fig. 2. The maximum values for β^2 are around 2000, matching expectations [10] and have uncertainties of 13 to 17%.

Table I: Summary of systematic uncertainties on $|g_{a\gamma}|$. Minimum and maximum uncertainties among the frequency range for all physics-runs are reported as first and second values (when necessary). The uncertainty from each physics-run is considered individually when included in the limit estimation.

Effect	Uncertainty in $\lvert g_{a\gamma}\rvert$
Y-factor power calibration	3% to 5%
Receiver chain power stability	$\leq 2\%$
Axion field – TE_{11} overlap	6%
Booster model parameters	3% to 6%
LNA impedance mismatch	$\leq 7\%$
Frequency stability of TE_{11} mode	$< 1\%$
Total	5% to 10%

Uncertainties in $|g_{a\gamma}|$ due to Y-factor calibration and β^2 determination are detailed in Table I.

Analysis— The analysis procedure for the MADMAX axion DM search [38] is modeled after the framework established by HAYSTAC [39] and adopts their nomenclature. It combines a set of individual power spectra $P_i(\nu)$, each measured with $\mathcal{O}(15\,\text{min})$ averaging time, to a *grand spectrum*, where the full axion signal information is contained in a single bin. The raw FFT data are re-binned for analysis to 0.9 kHz.

The spectra $P_i(\nu)$ are filtered using a fourth-order Savitzky-Golay (SG) filter [40] with a window length of $\sim$ 1 MHz to extract the baselines $P_{{\rm bl},i}(\nu)$, which are subsequently used to obtain the processed spectra $p_{{\rm proc},i} = (P_i/P_{{\rm bl},i} - 1)$. These processed spectra give local power excesses above the baseline across all frequency bins i. In the absence of an axion signal and assuming ideal baseline removal, the $p_{{\rm proc},i}$ are expected to follow Gaussian white noise with zero mean and a standard deviation determined by the averaging time. Studies of the full analysis chain applied to simulated data including

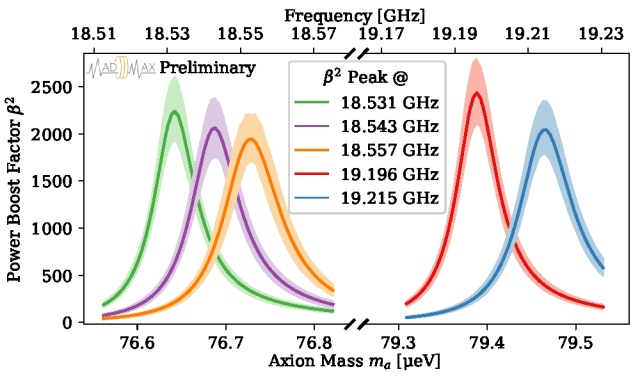

Figure 2: Modelled boost factor distributions for the five data-runs. Lines denote mean β^2 and shaded regions give $\pm 1\sigma$ intervals.

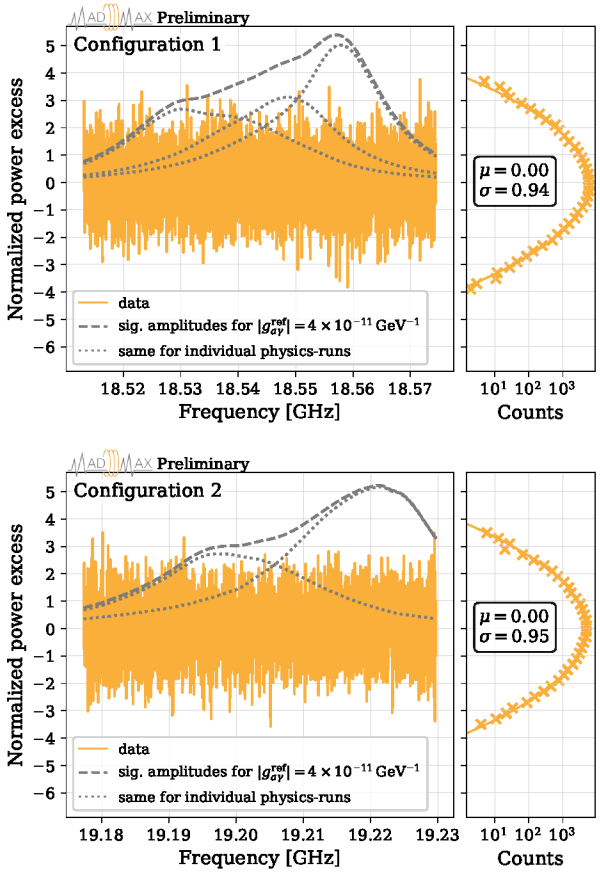

Figure 3: Grand spectra with 0.9 kHz bin-width for both booster configurations. Dashed grey lines indicate the envelope of expected amplitude in each frequency bin for a reference axion signal with photon coupling of $|g_{a\gamma}| = 4 \times 10^{-11}\,\mathrm{GeV}^{-1}$, combining all physics-runs for each configuration. Dotted lines show the expectation for individual physics-runs. The right panels display histograms of the spectra, overlaid with a best-fit Gaussian distribution with the indicated mean and standard deviation.

synthetic axion signals reveal an SNR attenuation due to the SG filter by a factor of $\eta_{\mathrm{SG}} = 0.92$, which is constant in the range $1 < \mathrm{SNR} < 10$.

The baseline of the recorded power spectra unexpectedly fluctuates on the scale of $\sim$ 9 kHz which introduces unwanted correlations between the processed spectra. This sinusoidal fluctuation is removed by applying a digital notch filter on the inverse Fourier transforms of the $P_i(\nu)$. The filter has negligible influence on both amplitude and line-shape of any potential axion signal, while being effective at eliminating the DAQ artefact. In combination with the SG filter, this process ensures uncorrelated $p_{\mathrm{proc},i}$. The $p_{\mathrm{proc},i}$ are scaled and combined using weights that take the axion sensitivity depending on the B-field strength in individual runs into account. The resulting combined spectrum is then cross-correlated with the expected axion line-shape [41, 42] to yield the grand spectrum. A local DM velocity dispersion $\sigma_v = 218\,\mathrm{km/s}$ [43] and a velocity of the laboratory relative to the DM halo $v_{\mathrm{lab}} = 242\,\mathrm{km/s}$ [44] are used.

The grand spectrum is unitless and, in the absence of an axion signal, expected from simulation to have zero mean and a standard deviation of 0.94. This value is now slightly below one due to correlations induced by the SG filter [39]. Grand spectra for both configurations are presented in Fig. 3. An axion signal at mass m_a would manifest as a narrow, localized excess at a frequency corresponding to m_a. Fig. 3 shows as grey dashed line the envelope of the expected amplitude of excesses, reflecting the SNR of an axion signal with $|g_{a\gamma}^{\mathrm{ref}}| = 4\times10^{-11}\,\mathrm{GeV}^{-1}$. Its frequency dependence is determined by a combination of T_{sys} and β^2. The largest grand spectrum excess observed in both configurations has a local significance of 3.9σ, which is consistent with statistical expectations. The probability of an equal or larger excess occurring across the entire dataset assuming no axion signal is $p = 0.13$.

Since no evidence of DM axions is found, an upper limit on the axion-photon coupling $|g_{a\gamma}|$ is derived at 95% Confidence Level (CL) for each 0.9 kHz bin as shown in Fig. 4. Systematic uncertainties from Table I are treated as independent and are propagated to $|g_{a\gamma}|$. The resulting limits on DM axions exceed previous results from the CAST helioscope [45] and astrophysical considerations [46].

Conclusion— Searching for axions with a dielectric haloscope, as proposed by the MADMAX collaboration, facilitates accessing the "heavy" axion mass region above $\sim$ 40 μeV favored by post-inflationary PQ-symmetry breaking scenarios. A novel boost factor determination method was developed and applied to derive first results from a prototype operated in CERN's Morpurgo magnet, using the intrinsic advantages offered by the MADMAX approach. Detailed understanding of the radio frequency response of a booster system with closed boundary conditions was demonstrated. The booster could be quickly tuned and re-calibrated to different frequencies demonstrating in principle the opportunity for future larger-range frequency scans. The data from the prototype test campaign using a small booster system inside a modest B-field allow to probe for axion dark matter in previously uncharted territory. The achievements presented here and in [35] provide a firm basis for the future research and development program towards a competitive dielectric haloscope, which will include the development of boosters with more and larger dielectric disks, the demonstration of the calibration and operation of boosters at cryogenic temperatures and the implementation of tuning mechanisms via motorized disk position controls [27, 32, 33]. With ongoing development of a future, unique, large-bore 9 T dipole magnet [31, 47], the MADMAX collaboration is on a very promising track towards probing dark matter QCD axions in the 100 μeV mass region.

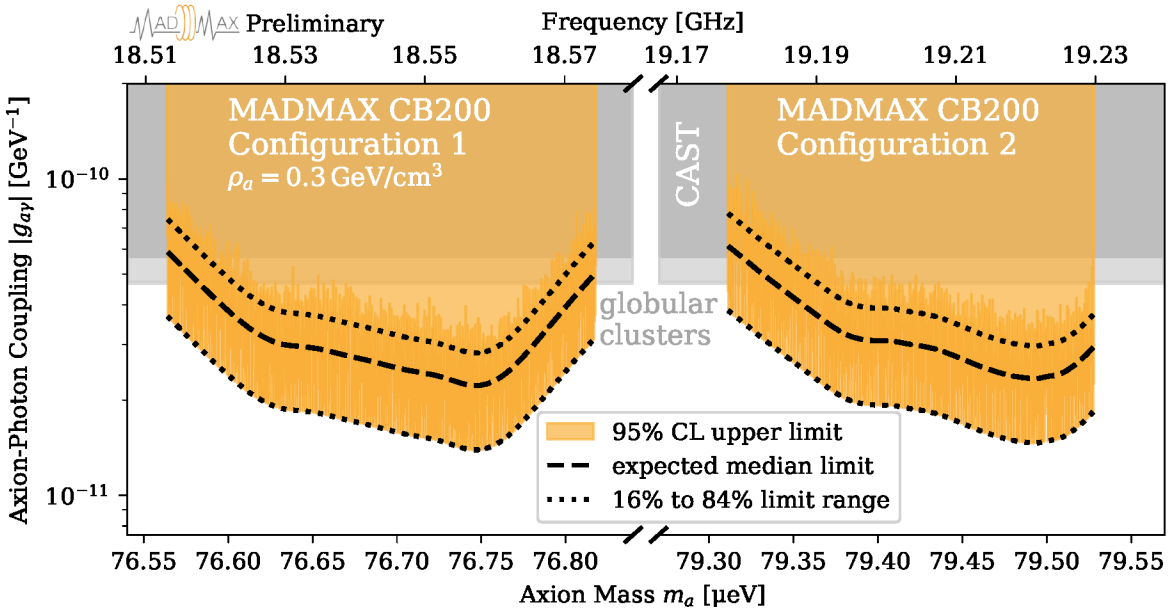

Figure 4: 95% CL exclusion limits in 0.9 kHz bins (orange) from the 2024 MADMAX axion search with the CB200 prototype using the Morpurgo magnet at CERN assuming a local axion DM density of $\rho_a = 0.3\,\mathrm{GeV\,cm^{-3}}$. Limits are compared to the helioscope experiment CAST [45] (dark grey) as well as to globular cluster limits [46] (light grey). The expected median limit and the 16% and 84% quantiles are shown as black dashed and lower and upper dotted lines, respectively. The limits are truncated below the 16% quantile. (A zoom into the most sensitive mass range is shown in Fig. S8 in suppl. material.)

Acknowledgements—The authors would like to thank the CERN central cryogenic laboratory and the CERN magnet team for the support during all the measurements with the Morpurgo magnet. We thank O. Reimann, D. Strom and A. Hambarzumjan for significant contributions during the first phase of the MADMAX project. We thank O. Rossel for providing the drawing of the setup and artistic support. We acknowledge support by the Helmholtz Association (Germany); Deutsche Forschungsgemeinschaft (DFG, German Research Foundation) under Germany's Excellence Strategy – EXC 2121 "Quantum Universe" – 390833306. Computations were performed with computing resources granted by RWTH Aachen University under project 7936. SK is supported by Fermi Research Alliance, LLC under Contract No. DE-AC02-07CH11359 with the U.S. Department of Energy, Office of Science, Office of High Energy Physics. We acknowledge the support of the MADMAX project by the Max Planck Society.

[1] I. G. Irastorza and J. Redondo, *New experimental approaches in the search for axion-like particles*, *Prog. Part. Nucl. Phys.* **102** (2018) 89 [1801.08127].

[2] L. F. Abbott and P. Sikivie, *A Cosmological Bound on the Invisible Axion*, *Phys. Lett. B* **120** (1983) 133.

[3] M. Dine and W. Fischler, *The Not So Harmless Axion*, *Phys. Lett. B* **120** (1983) 137.

[4] J. Preskill, M. B. Wise and F. Wilczek, *Cosmology of the Invisible Axion*, *Phys. Lett. B* **120** (1983) 127.

[5] R. D. Peccei and H. R. Quinn, *CP Conservation in the Presence of Pseudoparticles*, *Phys. Rev. Lett.* **38** (1977) 1440.

[6] R. D. Peccei and H. R. Quinn, *Constraints imposed by CP conservation in the presence of pseudoparticles*, *Phys. Rev. D* **16** (1977) 1791.

[7] S. Weinberg, *A new light boson?*, *Phys. Rev. Lett.* **40** (1978) 223.

[8] F. Wilczek, *Problem of Strong P and T Invariance in the Presence of Instantons*, *Phys. Rev. Lett.* **40** (1978) 279.

[9] M. Buschmann, J. W. Foster, A. Hook, A. Peterson, D. E. Willcox, W. Zhang et al., *Dark matter from axion strings with adaptive mesh refinement*, *Nature Commun.* **13** (2022) 1049 [2108.05368].

[10] A. J. Millar, G. G. Raffelt, J. Redondo and F. D. Steffen, *Dielectric Haloscopes to Search for Axion Dark Matter: Theoretical Foundations*, *JCAP* **01** (2017) 061 [1612.07057].

[11] P. Sikivie, *Experimental Tests of the Invisible Axion*, *Phys. Rev. Lett.* **51** (1983) 1415.

[12] ADMX collaboration, N. Du et al., *A Search for Invisible Axion Dark Matter with the Axion Dark Matter Experiment*, *Phys. Rev. Lett.* **120** (2018) 151301 [1804.05750].

[13] ADMX collaboration, C. Bartram et al., *Search for Invisible Axion Dark Matter in the 3.3–4.2 μeV Mass Range*, *Phys. Rev. Lett.* **127** (2021) 261803 [2110.06096].

[14] ADMX collaboration, C. Bartram et al., *Axion Dark Matter eXperiment around 3.3 μeV with Dine-Fischler-Srednicki-Zhitnitsky Discovery Ability*, 2408.15227.

[15] Y. Kim et al., *Experimental Search for Invisible Dark Matter Axions around 22 μeV*, *Phys. Rev. Lett.* **133** (2024) 051802 [2312.11003].

[16] CAPP collaboration, S. Ahn et al., *Extensive Search for Axion Dark Matter over 1 GHz with CAPP'S Main Axion Experiment*, *Phys. Rev. X* **14** (2024) 031023 [2402.12892].

[17] B. M. Brubaker et al., *First results from a microwave cavity axion search at 24 μeV*, *Phys. Rev. Lett.* **118** (2017) 061302 [1610.02580].

[18] HAYSTAC collaboration, L. Zhong et al., *Results from phase 1 of the HAYSTAC microwave cavity axion experiment*, *Phys. Rev. D* **97** (2018) 092001 [1803.03690].

[19] B. T. McAllister, G. Flower, J. Kruger, E. N. Ivanov, M. Goryachev, J. Bourhill et al., *The ORGAN Experiment: An axion haloscope above 15 GHz*, *Phys. Dark Univ.* **18** (2017) 67 [1706.00209].

[20] A. Quiskamp, B. T. McAllister, P. Altin, E. N. Ivanov, M. Goryachev and M. E. Tobar, *Exclusion of Axionlike-Particle Cogenesis Dark Matter in a Mass Window above 100 μeV*, *Phys. Rev. Lett.* **132** (2024) 031601 [2310.00904].

[21] A. P. Quiskamp, G. Flower, S. Samuels, B. T. McAllister, P. Altin, E. N. Ivanov et al., *Near-quantum limited axion dark matter search with the ORGAN experiment around 26 μeV*, 2407.18586.

[22] J. Jaeckel and J. Redondo, *Resonant to broadband searches for cold dark matter consisting of weakly interacting slim particles*, *Phys. Rev. D* **88** (2013) 115002 [1308.1103].

[23] A. Caldwell, G. Dvali, B. Majorovits, A. Millar, G. Raffelt, J. Redondo et al., *Dielectric Haloscopes: A New Way to Detect Axion Dark Matter*, *Phys. Rev. Lett.* **118** (2017) 091801 [1611.05865].

[24] MADMAX collaboration, P. Brun et al., *A new experimental approach to probe QCD axion dark matter in the mass range above 40 μeV*, *Eur. Phys. J. C* **79** (2019) 186 [1901.07401].

[25] D. Horns, J. Jaeckel, A. Lindner, A. Lobanov, J. Redondo and A. Ringwald, *Searching for WISPy Cold Dark Matter with a Dish Antenna*, *JCAP* **04** (2013) 016 [1212.2970].

[26] S. Knirck, J. Schütte-Engel, A. Millar, J. Redondo, O. Reimann, A. Ringwald et al., *A First Look on 3D Effects in Open Axion Haloscopes*, *JCAP* **08** (2019) 026 [1906.02677].

[27] J. Egge, S. Knirck, B. Majorovits, C. Moore and O. Reimann, *A first proof of principle booster setup for the MADMAX dielectric haloscope*, *Eur. Phys. J. C* **80** (2020) 392 [2001.04363].

[28] MADMAX collaboration, S. Knirck et al., *Simulating MADMAX in 3D: requirements for dielectric axion haloscopes*, *JCAP* **10** (2021) 034 [2104.06553].

[29] J. Egge, *Axion haloscope signal power from reciprocity*, *JCAP* **04** (2023) 064 [2211.11503].

[30] J. Egge et al., *Experimental determination of axion signal power of dish antennas and dielectric haloscopes using the reciprocity approach*, *JCAP* **04** (2024) 005 [2311.13359].

[31] C. Lorin, W. A. Maksoud, J. Allard, C. Berriaud, V. Calvelli, L. Denarie et al., *Development, integration, and test of the macqu demo coil toward madmax quench analysis*, *IEEE TAS* **33** (2023) 1.

[32] E. Garutti, H. Janssen, D. Kreikemeyer-Lorenzo, C. Krieger, A. Lindner, B. Majorovits et al., *Qualification of piezo-electric actuators for the MADMAX booster system at cryogenic temperatures and high magnetic fields*, *JINST* **18** (2023) P08011 [2305.12808].

[33] MADMAX collaboration, B. Ary Dos Santos et al., *First mechanical realization of a tunable dielectric haloscope for the MADMAX axion search experiment*, 2407.10716.

[34] R. Cervantes et al., *ADMX-Orpheus first search for 70 μeV dark photon dark matter: Detailed design, operations, and analysis*, *Phys. Rev. D* **106** (2022) 102002 [2204.09475].

[35] MADMAX collaboration, J. Egge et al., *First search for dark photon dark matter with a MADMAX prototype*, 2408.02368.

[36] D. Pozar, *Microwave Engineering*. Wiley, 2011.

[37] M. Morpurgo, *A large superconducting dipole cooled by forced circulation of two phase helium*, *Cryogenics* **19** (1979) 411.

[38] J. Diehl, *Statistical Methods for a First MADMAX Axion Dark Matter Search and Beyond*, Ph.D. thesis, Technical University Munich, 2024.

[39] B. M. Brubaker, L. Zhong, S. K. Lamoreaux, K. W. Lehnert and K. A. van Bibber, *HAYSTAC axion search analysis procedure*, *Phys. Rev. D* **96** (2017) 123008 [1706.08388].

[40] A. Savitzky and M. J. E. Golay, *Smoothing and differentiation of data by simplified least squares procedures*, *Analytical Chemistry* **36** (1964) 1627.

[41] C. A. J. O'Hare and A. M. Green, *Axion astronomy with microwave cavity experiments*, *Phys. Rev. D* **95** (2017) 063017 [1701.03118].

[42] J. Diehl, J. Knollmüller and O. Schulz, *Bias-free estimation of signals on top of unknown backgrounds*, *Nucl. Instrum. Meth. A* **1063** (2024) 169259 [2306.17667].

[43] J. Bovy, C. Allende Prieto, T. C. Beers, D. Bizyaev, L. N. da Costa, K. Cunha et al., *The Milky Way's Circular-velocity Curve between 4 and 14 kpc from APOGEE data*, *Astrophys. J.* **759** (2012) 131 [1209.0759].

[44] K. Malhan, R. A. Ibata and N. F. Martin, *Measuring the Sun's velocity using Gaia EDR3 observations of Stellar Streams*, 2012.05271.

[45] CAST collaboration, K. Altenmüller et al., *A new upper limit on the axion-photon coupling with an extended CAST run with a Xe-based Micromegas detector*, 2406.16840.

[46] M. J. Dolan, F. J. Hiskens and R. R. Volkas, *Advancing globular cluster constraints on the axion-photon coupling*, *JCAP* **10** (2022) 096 [2207.03102].

[47] A. Torre and L. Quettier, *Editorial of the MADMAX Special Section*, *IEEE TAS* **33** (2023) 1.

[48] https://www.keysight.com/de/de/products/software/pathwave-design-software/pathwave-advanced-design-system.html

Supplemental Material for the Letter
First search for axion dark matter with a MADMAX prototype

In this Supplemental Material, we provide further figures with additional information.

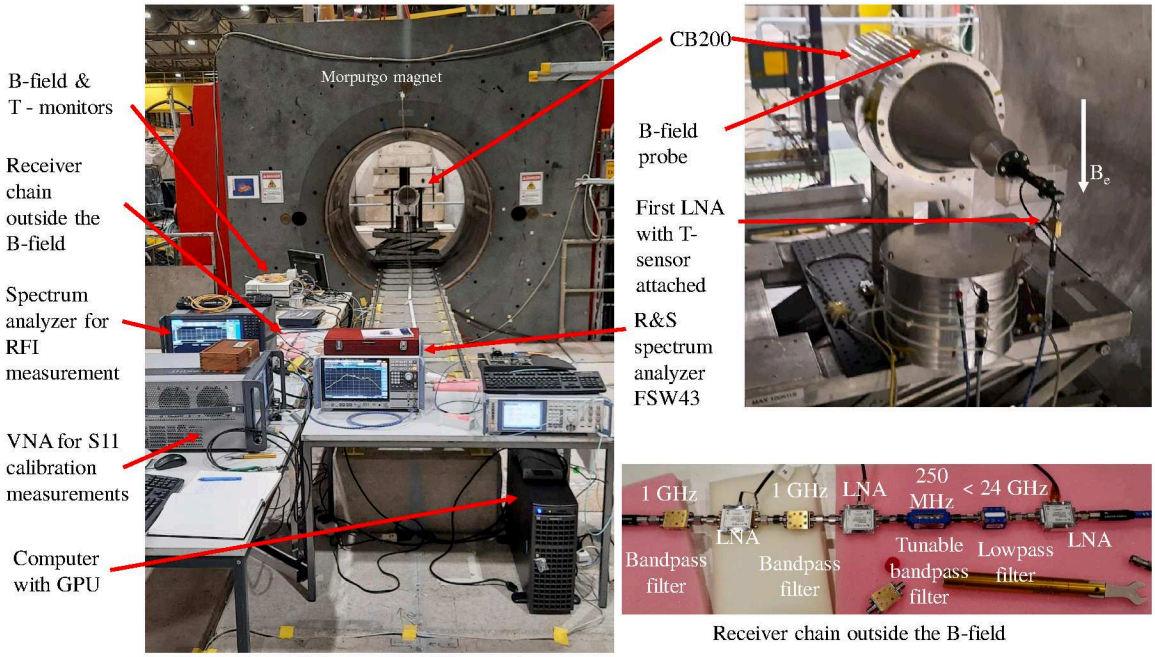

Receiver chain outside the B-field

Figure S1: Left and top right: Picture of CB200 inside the Morpurgo magnet and equipment for data taking and data monitoring. Bottom right: Receiver chain components outside the B-field.

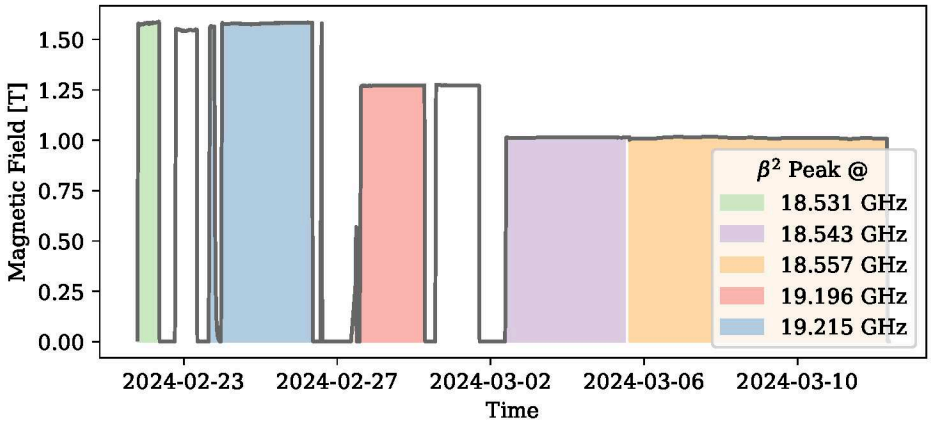

Figure S2: Time evolution of the available magnetic field strength. Individual physics-runs are denoted with various colors. Due to issues encountered with the cryogenic system of the magnet after first measurements at 1.6 T the field strength had to be reduced to 1.3 T and ultimately to 1.0 T. Two time periods have not been used for physics measurements (white). For the first time period test measurements were conducted with a different receiver system. During the second time period the booster peak frequency displayed significant variation over time.

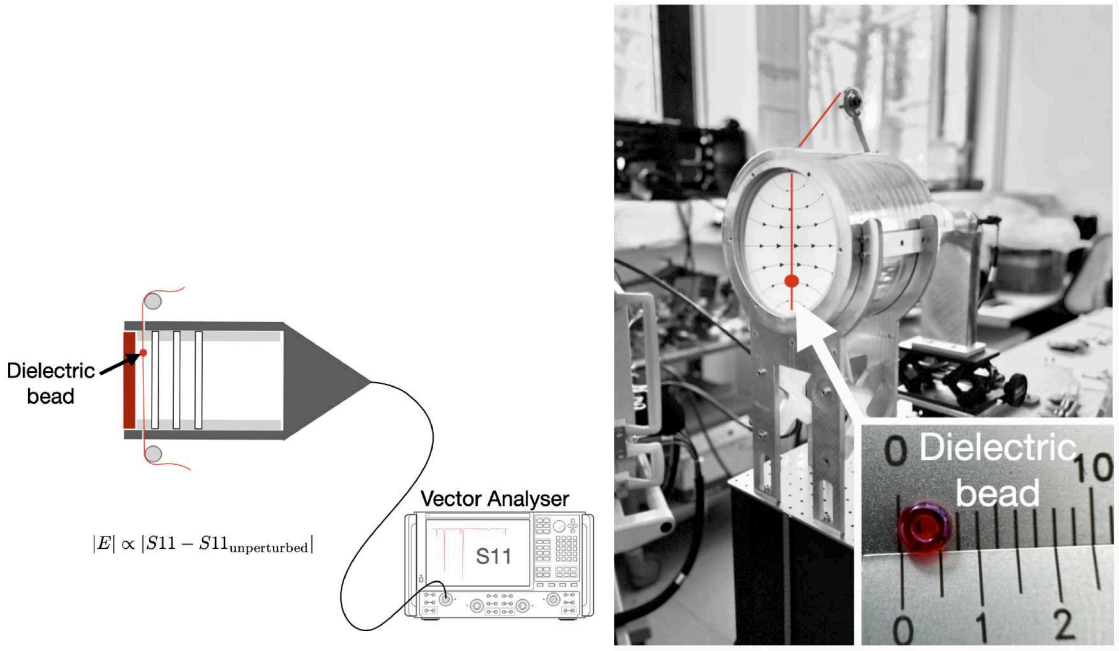

Figure S3: The field distribution inside the booster can be spatially resolved via the bead-pull method [30]: A small dielectric bead is pulled along the transversal profile of the booster. The bead introduces small perturbations proportional to the electric field strength at the bead's position. A set of perturbed reflectivity measurements (complex S_{11} parameter) is obtained for each bead position using Vector Network Analyser (VNA). Such bead-pull measurements were conducted to verify the field distribution for all booster configurations.

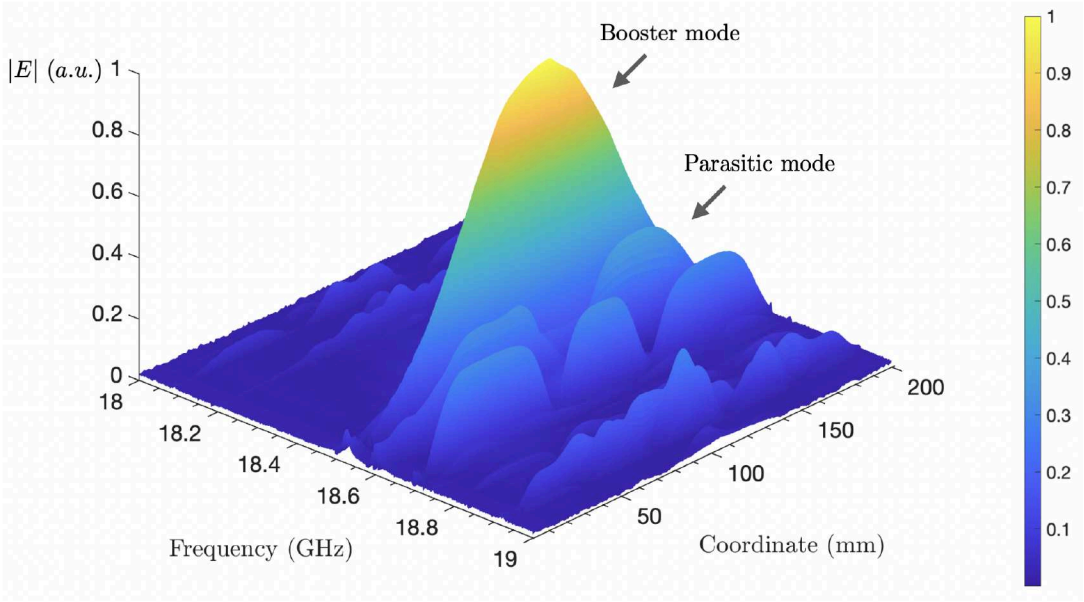

Figure S4: Measured distribution of the electric field obtained along the diameter of the booster as a function of frequency, from 18 to 19 GHz. The center is at coordinate 100 mm. The field profile of the booster mode shows a well-defined single peak, as expected for the intended TE_{11} mode. The measurement allows to identify higher-order parasitic modes as indicated. From the deviation between measured and expected shape of the TE_{11} booster mode the uncertainty on the overlap integral between TE_{11} mode and the uniform axion current can be derived.

Table S1: Summary of the physics-runs used in the analysis.

$f(\max\ \beta^2)$ [GHz]	measurement time [h]	median B field [T]
18.531	13.5	1.58
18.543	73.75	1.01
18.557	159.0	1.01
19.196	40.75	1.27
19.215	61.25	1.58

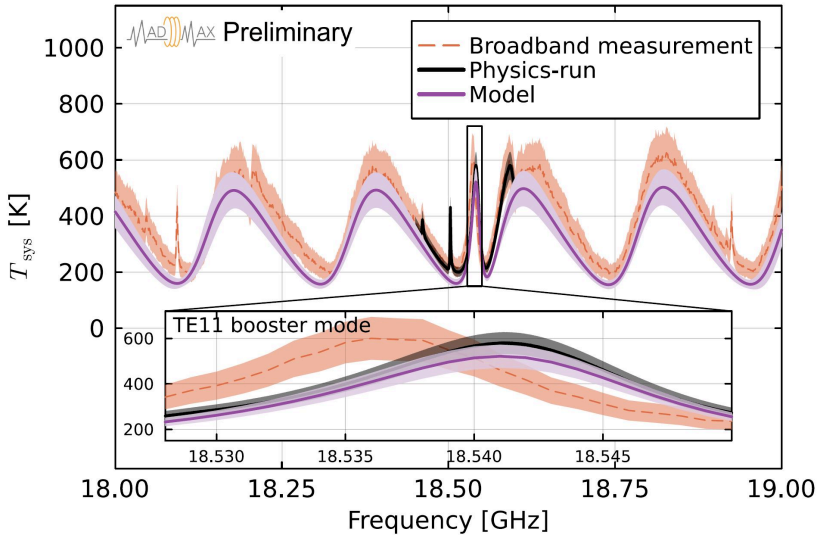

Figure S5: Exemplary system temperature spectra (T_{sys}) obtained from broadband measurements (dashed red) and a power spectrum from an axion physics-run (solid black). For the latter, only a reduced frequency range around the TE_{11} mode resonance is recorded. The T_{sys} spectrum obtained from the booster model (solid magenta) is superimposed with the band around the line indicating the systematic uncertainties. For the broadband measurements, the model describes well the standing wave pattern induced by the amplifier noise ($\sim 230\,\mathrm{K}$, see text) inside the booster, but not the fine structures indicating the limitation of the one-dimensional model. For the physics-run power spectrum, a zoom to the TE_{11} booster mode region is shown in the inset and a good agreement with the model is observed. The shift of the TE_{11} resonance peak frequency between broadband and physics spectrum can be attributed to environmental effects, specifically the tuning mechanism being affected during magnet ramp up/down – the shift shown is the biggest observed in all datasets. To match the resonance position of the physics-run measurement after the system stabilized, the distance between mirror and closest disk used in the booster model was adjusted, requiring O(µm) changes from the previously determined parameters.

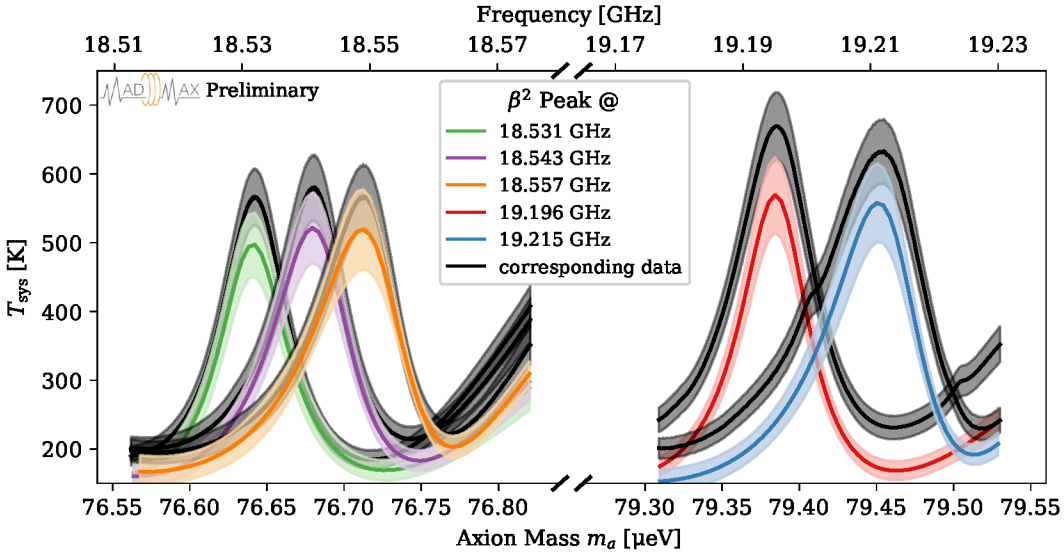

Figure S6: Simulation and data for each physics-run's power spectrum around the TE_{11} booster mode. The model reproduces the frequency position of the resonance peak. System temperature is consistently slightly underestimated, which does not affect the boost factor determination, as only the frequency dependence of T_{sys} is used in the analysis.

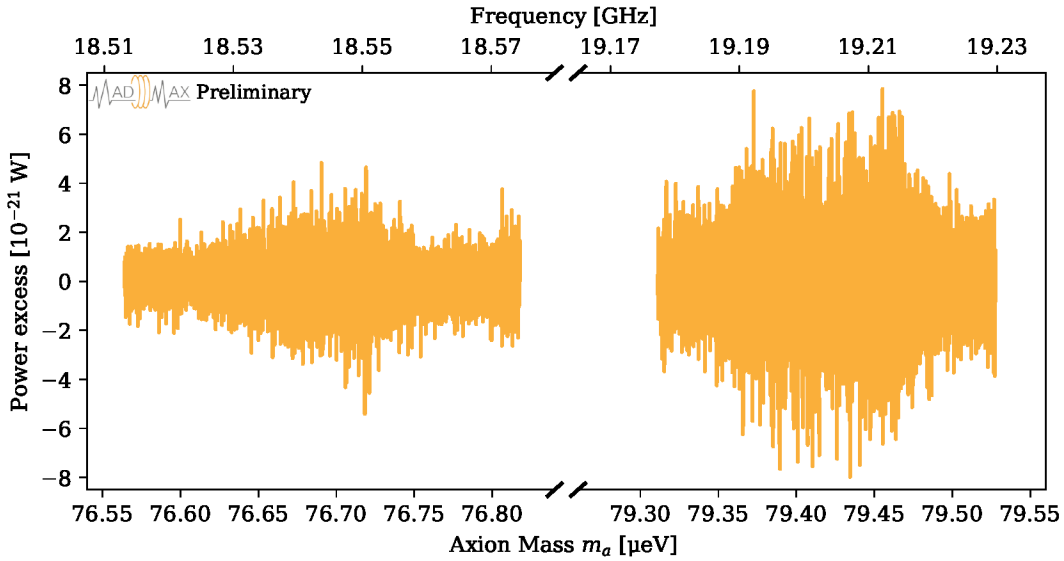

Figure S7: Observed cross-correlated power excess as a function of frequency.

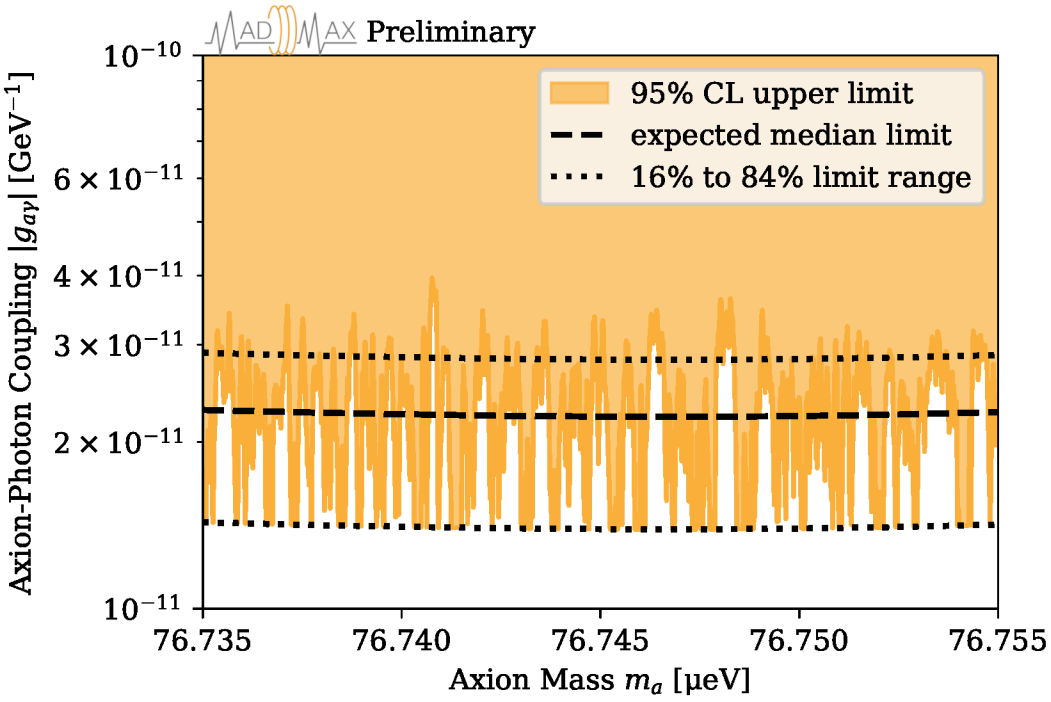

Figure S8: 95% CL exclusion limit around the most sensitive region for configuration 1. The bin to bin fluctuation of the limits and the truncation below the 16% quantile are clearly visible, as are correlations between adjacent frequency bins. The latter arise due to cross-correlation with the axion lineshape as mentioned in the text.